UCRL-JC-118290
PREPRINT

# MID-IR DETECTION: DETECTOR CIRCUITRY AND NOISE

Asher Blum, Alan Gates, Mario Montoya, and Richard Wyeth

Lawrence Livermore National Laboratory
Livermore, CA 94551

This paper was prepared for
the Proceedings of the 1994 CALIOPE ITR Conference
held May 26-28, 1994, in Livermore, California

July 1994

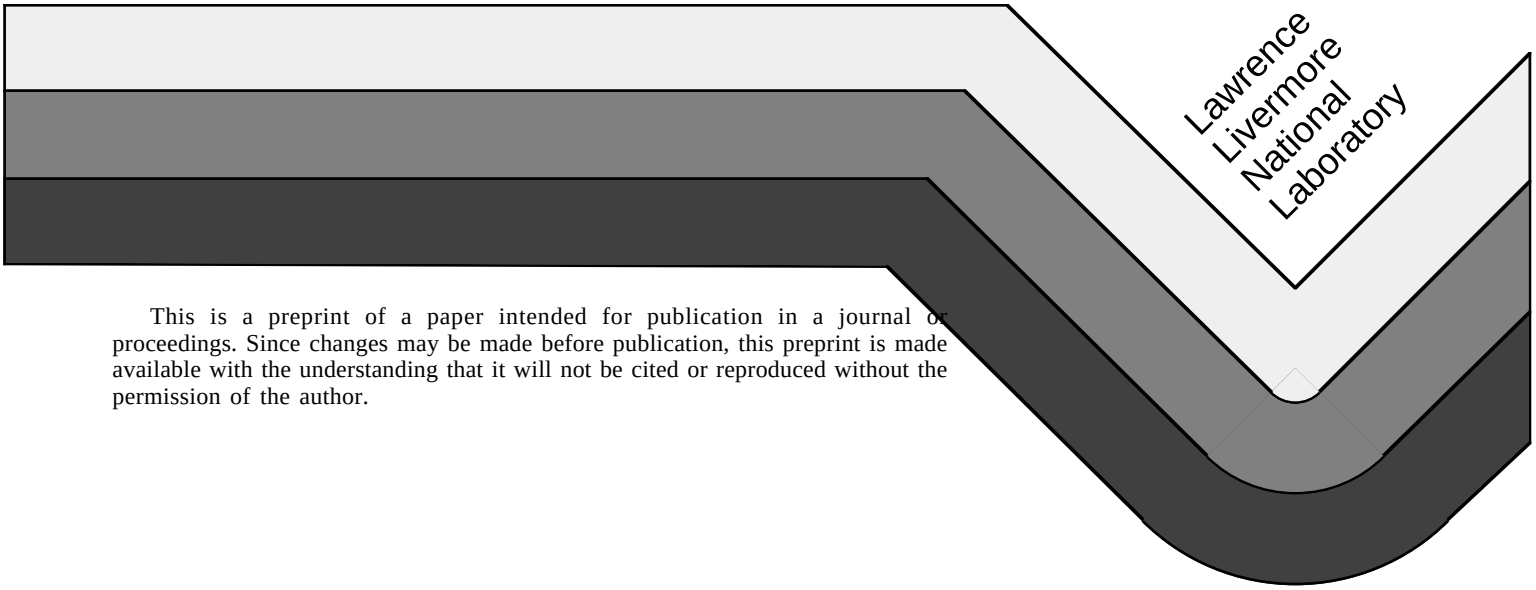

# MID-IR DETECTION: DETECTOR CIRCUITRY AND NOISE

*Asher Blum, Alan Gates, Mario Montoya, and Richard Wyeth*
*Lawrence Livermore National Laboratory, Livermore, California 94551*

## Introduction

Our ability to measure the spectral transmission of the atmosphere is limited in two ways. First, by noise that is added to the returning signal by random processes such as electronic noise and the random emission of IR photons. Second, by speckle that acts as a wavelength dependent multiplier of the returning signal amplitude. In this paper we report our estimates of the effects of added random noise on the measurements planned for the October field tests. We do not consider speckle which is fundamentally different from "additive noise" and is being separately considered by others.

The system which will be fielded by LLNL in October '94 will transmit on and off resonance wavelengths λ1 and λ2. The integral of the returning signal as well as an integral of the transmitted signal will be recorded at each wavelength. From these the transmission can be calculated. The two returning wavelengths are separated in a spectrograph and sent to detectors in a 16-element array. Each detector is followed by an amplifier. This is illustrated in Figure 1.

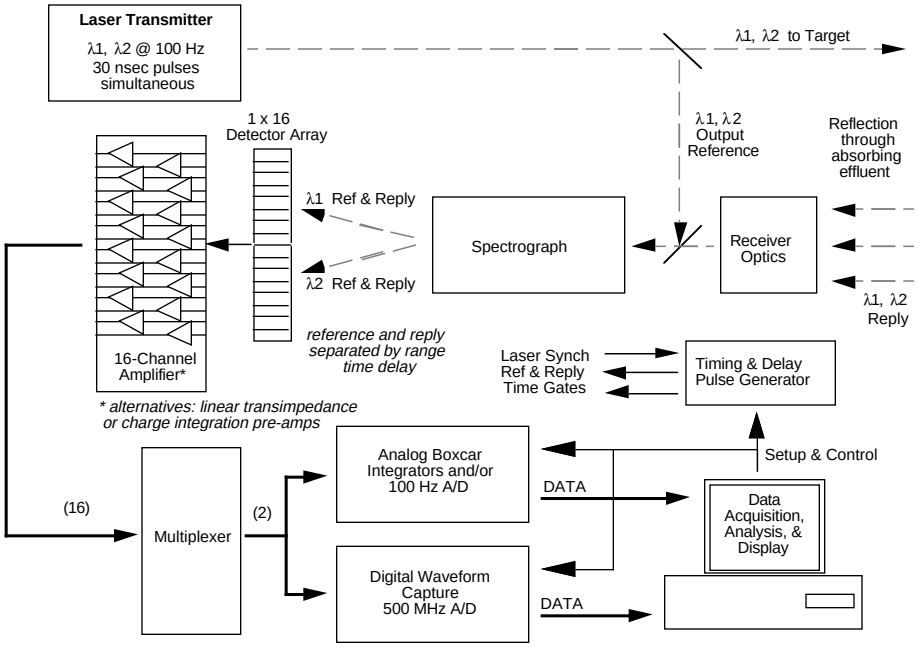


**Figure 1.** CALIOPE DIAL block diagram.

To maintain good system linearity, nominally constant detector voltage, and large dynamic range, it is desirable that the amplifier input be a virtual ground. Either a linear transimpedance amplifier or negative feedback charge sensitive can satisfy this requirement. Two of the 16 amplifier outputs are selected by a multiplexer and passed to data processing and/or recording hardware. The charge sensitive amplifier integrates the arriving current and we need only record its output. The digital sampling (waveform capture) hardware can be used in a mode in which it records the integrated outputs. The

linear transimpedance amplifier output must be integrated and Figure 1 shows two possible options for accomplishing this. First, a boxcar integrator provides an analog option. Second, we can digitally sample the signal and use a computer to sum the samples. We will compare the noise which we predict for the charge sensitive amplifier (which is under construction, but has not yet been built) with measurements of the transimpedance amplifier performance.

Measurement errors arise from a variety of sources. Figure 2 displays a list of possible sources of error. Some of these are reduced by the argument that both the on and off resonance wavelengths are equally affected (target reflectivity and propagation excluding speckle) and ultimately only their ratio is important, some are reduced by the small time intervals between on and off resonance measurements (turbulence and target motion), and some are reduced by the normalization of the returning signal by a sample of the transmitted signals (laser energy). We do not consider these terms. As mentioned above we consider only additive noise: photon noise due to the background flux and thermal electronic noise.

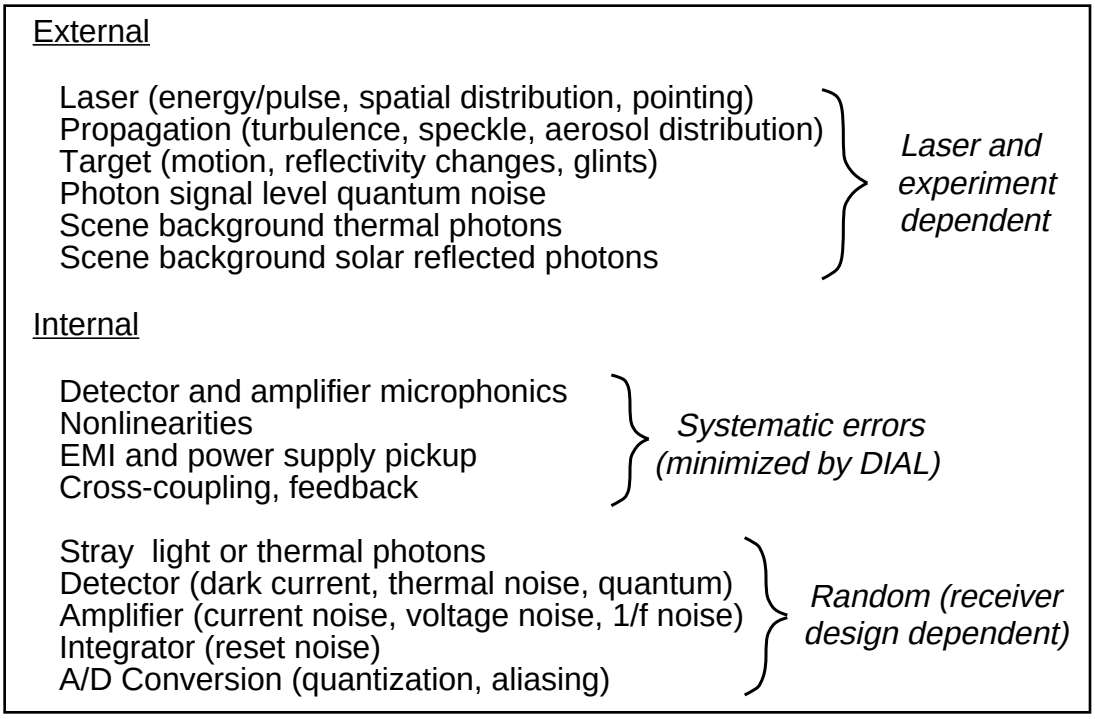


**Figure 2.** CALIOPE DIAL receiver - noise and error sources.

Assuming 1 mJ of transmitted laser energy, and the parameters (500 m, reflectivity of 0.5) given in Figure 3, we can compute the returned photons. Of those, some fraction will enter the slit which is assumed to be opened to the point at which the edges of the point spread functions just touch. Further reductions occur because of the spectrograph efficiency, cold filter transmission (0.5) and quantum efficiency of the detector. The photon fluxes at various points in the system are plotted in Figure 4. The same figure shows the thermally generated background current and the nominal solar generated flux. The signal photons arrive during a brief 30 ns interval and consequently generate a large peak current that is much higher than the steady state background.

Laser Transmitter
- Pulse Rate: 100 Hz
- Pulsewidth: 30 nanoseconds
- Wavelength (λ): 3.6 μmeter
- Spectral Format - two colors: λ1, λ2
- Separation ( | λ1–λ2 | ): 30 GHz
- Beam Divergence: 1 milliradian

Target
- Range: 500 meters
- Reflectivity: diffuse Lambertian@ 50%
- Type: Flat, captures entire 50 cm beam

Atmosphere
- Off-line Transmission: 95%
- On-line Effluent Absorption: 10 % max

Receiver Optics
- Aperture: 25 cm
- Focal Length: 1.75 meters
- Transmission: 0.8

Spectrometer
- Type: Grating
- Slit Width: 200 μmeter
- Optics Transmission: 0.5
- Wavelength Scale: 30 GHz/detector

Detector
- Type: photovoltaic InSb
- Cooling: liquid nitrogen pour-fill dewar
- Format: 16 element linear array
- Element Dimensions: 250 X 800μm
- Element Spacing: 275μm

Detector (continued)
- Quantum Efficiency: > 0.75
- Cold Stop Solid Angle: f/3.5
- Dark Current: 1 microampere
- Element Capacitance@0.3V bias: 20 pf
- Detector Parallel Resistance: > 1E7 ohms
- Detector Series Resistance: 200ohms

Detector Amplifier
- Types: wide bandwidth linear for post-integrator; charge amplifier with reset for direct integration
- Signal/Noise Ratio: 500 minimum

Post-Integrator
- Gate time: 50-200 nanoseconds
- Sensitivity: Variable with < 1 mv of noise and maximum output of several volts

D/A Converter
- Resolution: 12 bit
- Input range: -10V to +10V
- Mode: external synch, baseline subtraction
- Channels: 8 I/O channels, 2 synch inputs

Waveform Digitizer
- Resolution: 8-bit
- Sample rate: 1 Gsample/sec total
- Channels: 1-4
- Modes: waveform math including subtractiion, integration, averaging, etc.
- Internal waveform storage: 50 KBytes
- Data transfer rate: 1 Megabyte/sec

**Figure 3.** CALIOPE DIAL receiver-October, 1994 test configuration.

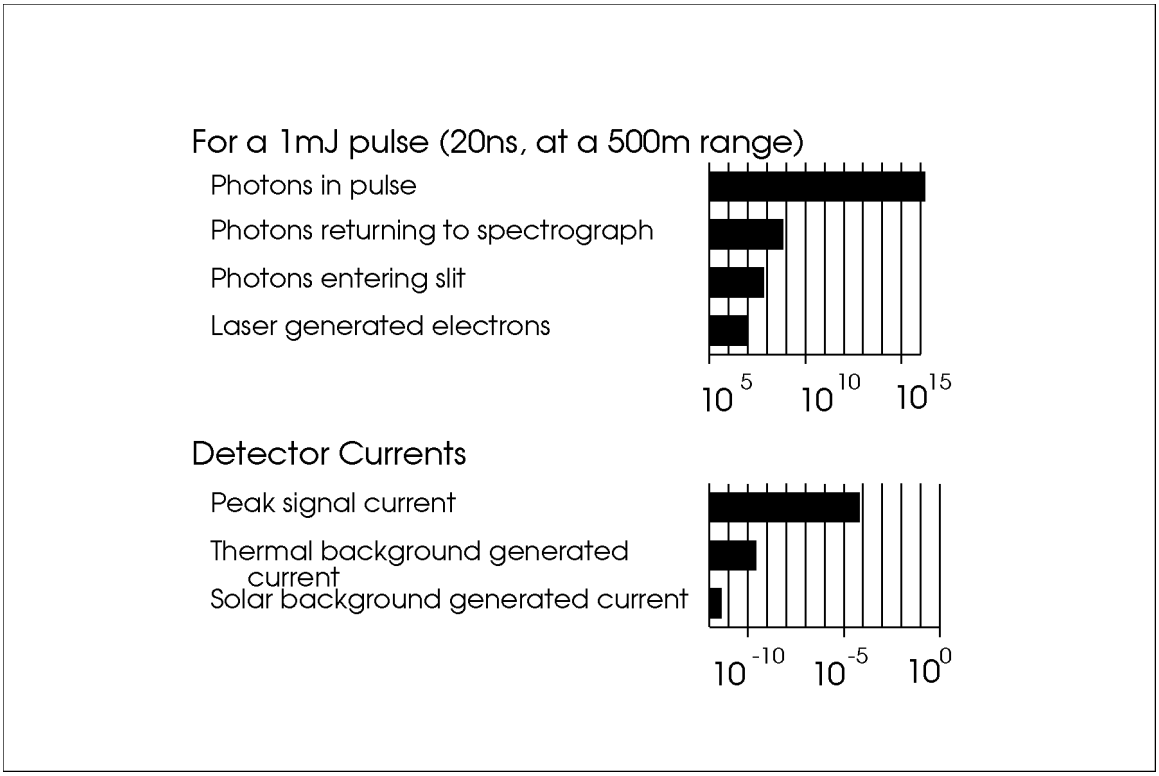


**Figure 4.** Background IR sources are weak compared to the returning laser signal.

## Amplifiers

Each of the amplifiers that we have considered offers certain advantages and disadvantages. The transimpedance amplifier followed by a fast sampling system can preserve a bandwidth-limited description of the temporal behavior of the signal. This allows a range of post-processing procedures to improve the measurement. For example, one can locate the signal's time of arrival and limit the integration to a narrow time window. In addition there is none of the reset noise from which analog integrators normally suffer. The charge sensitive amplifier has lower noise bandwidth but must integrate for a longer interval. Because it integrates the signal, less data is reported and the system will operate at higher pulse repetition rates with smaller storage requirements.

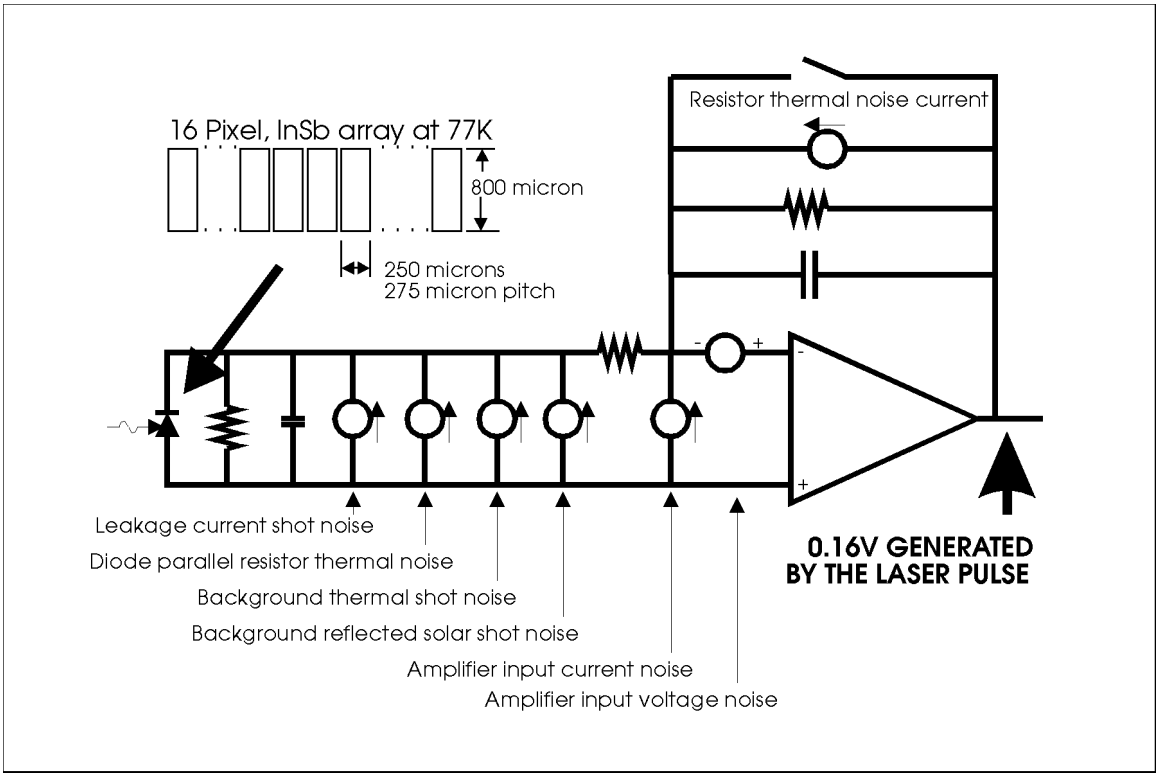


**Figure 5.** Charge sensitive amplifier with noise sources.

## Charge Sensitive Amplifier

The detector array consists of 800 micron by 250 micron p-n junctions as pictured in Figure 5 along with the charge sensitive amplifier and its noise sources.

The background reflected solar and thermal photon fluxes generate photon or shot noise. As listed in Figure 6, the reflected solar shot noise has a power spectral density of $1.1 \times 10^{-15}$ A / $\sqrt{\text{Hz}}$; the background thermal shot power spectral density is $8.1 \times 10^{-15}$ A / $\sqrt{\text{Hz}}$.

The detectors contribute two sources of noise. The dark current is $1.0 \times 10^{-10}$ A which results in a power spectral density of $5.6 \times 10^{-15}$ A / $\sqrt{\text{Hz}}$. The incremental resistance of the diode is $1.0 \times 10^{-9}$ ohms which results in a power spectral density of $2.1 \times 10^{-15}$ A / $\sqrt{\text{Hz}}$.

| Noise source | Key parameter | Power spectral density (1 sided) | Amplifier MS output | Sampler MS output |
|---|---|---|---|---|
| Leakage current shot noise | $I_{leak} = 10^{-10}$ A | $2qI_{leak} = 3.2\times10^{-29}$ A²/Hz | $2.5\times10^{-12}$ V² | $1.2\times10^{-13}$ V² |
| Detector thermal noise | $R_{det} = 10^{9}$ Ohm | $4kT/R_{det} = 4.3\times10^{-30}$ A²/Hz | $3.4\times10^{-13}$ V² | $1.6\times10^{-14}$ V² |
| Bkgrnd thermal shot noise | $I_{bk,T} = 2.06\times10^{-10}$ A | $2qI_{bk,T} = 6.6\times10^{-29}$ A²/Hz | $5.3\times10^{-12}$ V² | $2.4\times10^{-13}$ V² |
| Background reflected solar shot noise | $I_{bk,S} = 3.95\times10^{-12}$ A | $2qI_{bk,S} = 1.3\times10^{-30}$ A²/Hz | $1.0\times10^{-13}$ V² | $4.8\times10^{-15}$ V² |
| Amplifier input current noise | Manufacturer's spec | $= 4\times10^{-24}$ A²/Hz | $3.2\times10^{-7}$ V² | $1.5\times10^{-8}$ V² |
| Feedback resistor thermal noise current | $R_f = 4\times10^{6}$ Ohm | $4kT/R_f = 4.1\times10^{-27}$ A²/Hz | $3.3\times10^{-10}$ V² | $1.5\times10^{-11}$ V² |
| Amplifier input voltage noise | Manufacturer's spec | $= 1.6\times10^{-17}$ V²/Hz | $6.6\times10^{-9}$ V² | $2.8\times10^{-8}$ V² |

**Figure 6.** Chart of noise source amplitudes.

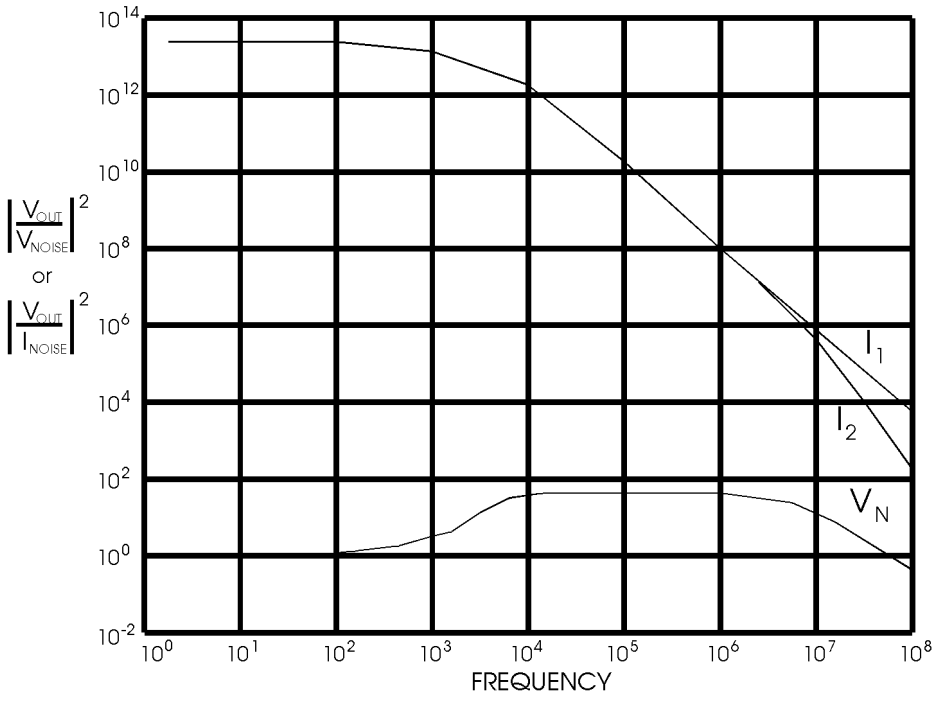


**Figure 7.** Power transfer functions.

These four current noise sources all are located at the same point in the circuit and consequently have the same power transfer function ( | output voltage / input current |$^2$ ). The power spectra of these sources (in $A^2$/Hz) can be summed to give a combined noise power spectrum. At each frequency the noise power spectrum is multiplied by the power transfer function to yield an output noise power spectrum. The power transfer function is calculated by conventional network analysis and is shown in Figure 7 where it is labeled as $I_1$.

This procedure can be repeated for the amplifier input current noise and the feedback resistor current noise. Because these are located at a different point in the network than the previous four noise sources, they connect to the output voltage by a slightly different power transfer function. This transfer function is labeled as $I_2$ in Figure 7.

The circuit of Figure 5 contains one more noise source, the amplifier input voltage noise. This is connected to the output voltage by the curve labeled $V_N$ in Figure 7.

At a selected time following the arrival of the return signal, we sample the integrator output. The integral of an output power spectra is the mean–square fluctuation of that sample. We can repeat this for the three output spectra and sum the results. Alternatively we can sample in more complex patterns. Figure 8 shows an example in which we sample three times: 1) 500 ns before the event interval which is the period of time during which we expect the return signal to arrive and which also is 500 ns long; 2) immediately before the event interval; and 3) immediately following the event interval. By adding the first and third samples and subtracting 2 times the second, we effectively multiply the power transfer functions of Figure 7 by the transfer functions of Figure 9. The result is shown in Figure 10. Note that the rapid variation at high frequencies due to sampling has not been shown in detail. We can now multiply the transfer functions of Figure 10 by the respective power spectral densities of the noise sources discussed above and integrate. At high frequencies we used the average value of the sampler transfer function. The triple sampling illustrates how 1/f noise can be reduced by multiple sampling.

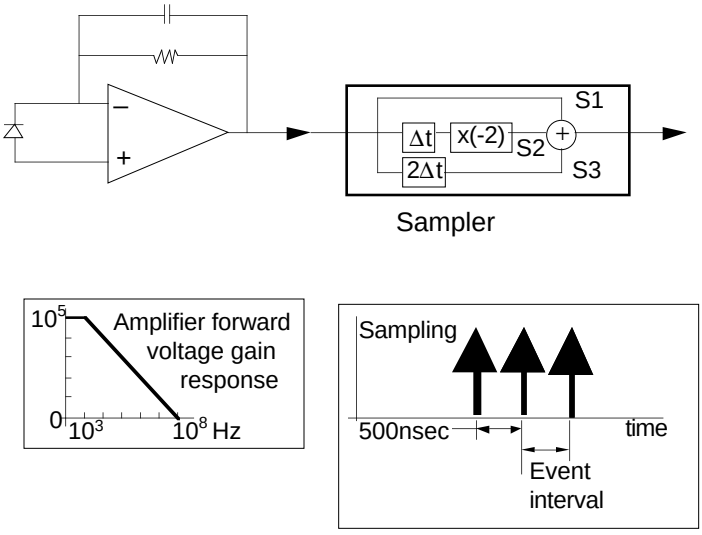


**Figure 8.** Block diagram of proposed sampling procedure.

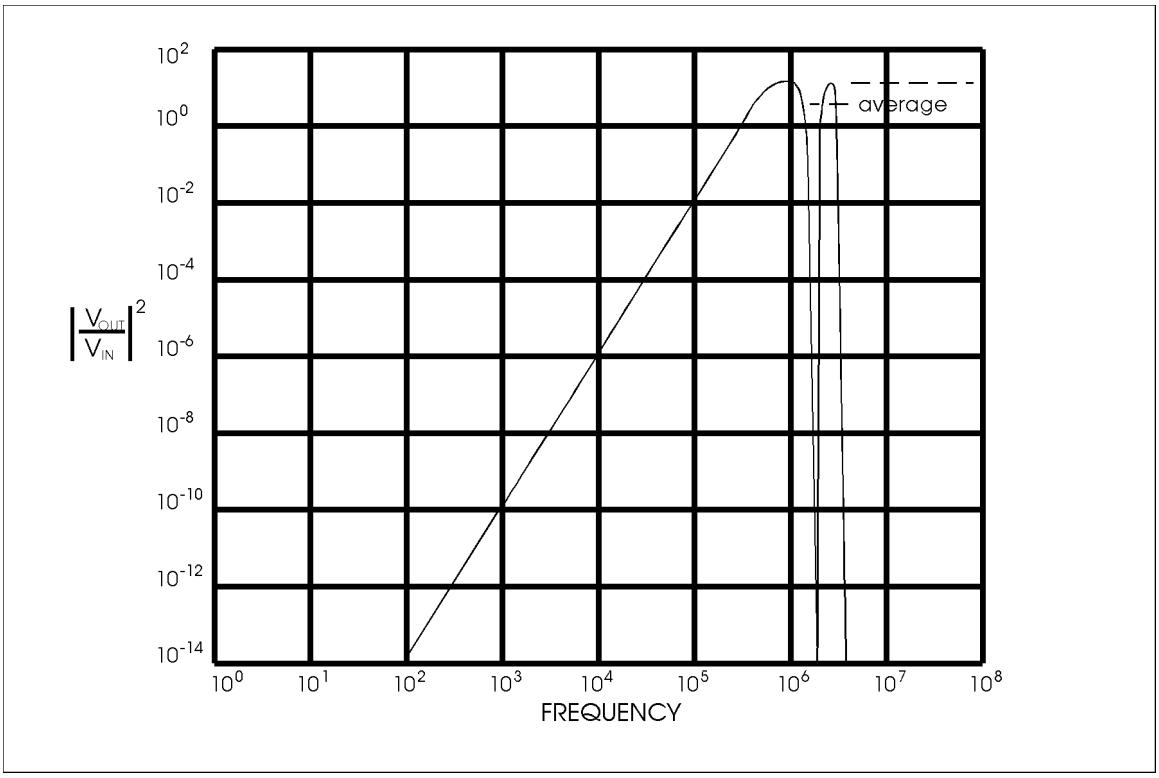


**Figure 9.** Power transfer function of sampling process.

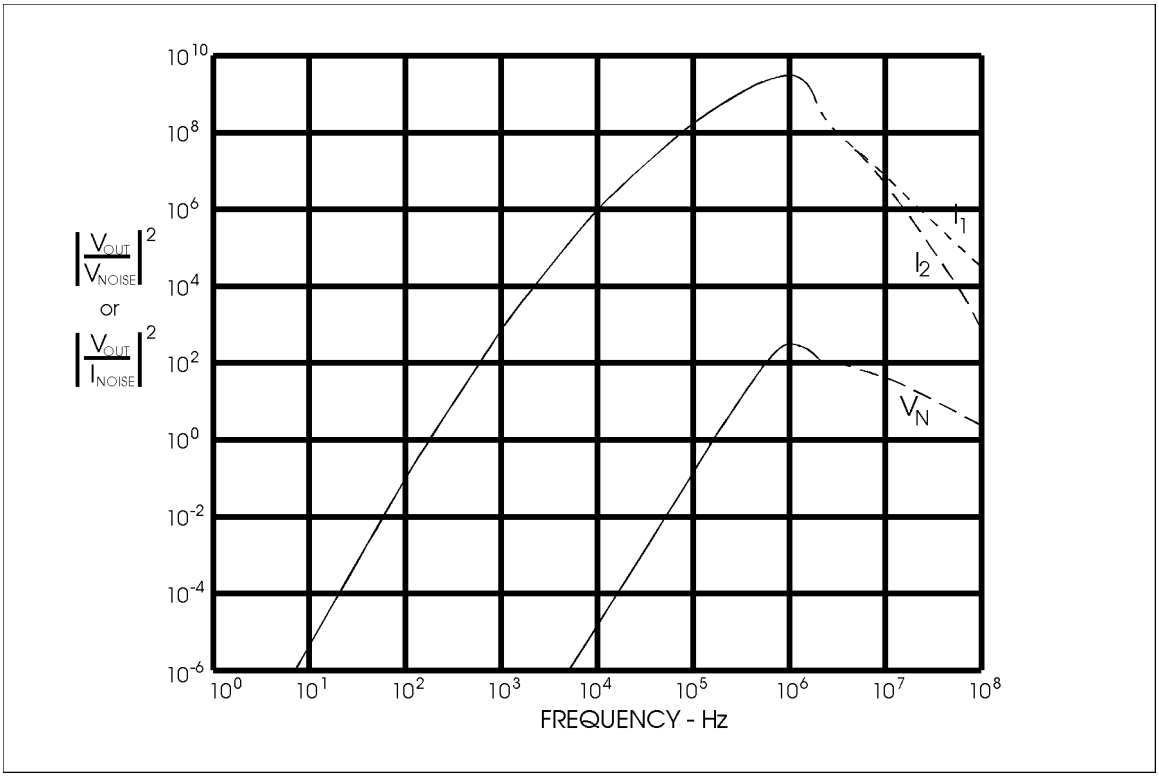


**Figure 10.** Power transfer function at sampler output.

The noise contributions with a single sample and with the triple sampling described in Figure 8 are shown in Figure 11 where they are shown as white and black bars respectively. Figure 11 shows that the amplifier noise dominates. Note that we have omitted the signal shot noise. If as shown in Figure 3, the signal generates $10^7$ electrons and results in 0.16 V at the output, we would expect a mean square fluctuation of $2.5 \times 10^{-9}$ $V^2$ due to an electron fluctuation of $\sqrt{10^7}$. This at least a factor of 10 below the amplifier noise contribution.

We have added the separate noise power contributions to estimate the output noise in the single sample and multiple sample cases. The results are shown in Figure 12. We conclude that one mJ transmitted will give us a single–to–noise ratio (S/N) of approximately 300 in the single sample case and 800 in the multiple sample case. Because the amplifier is far from saturated, increases in laser power will increase S/N. The analysis does not show the behavior of 1/f noise, but an additional benefit of multiple sampling is that it can be used to suppress 1/f noise as shown by the transfer function in Figure 9. This result is for one laser shot. Averaging over many measurements is expected to yield the usual square root of the number of samples improvement.

We conclude that due to the amplifier and detector noise sources, one mJ of laser light will result in S/N values between 300 for a singly sampled output and 800 for a triply sampled output.

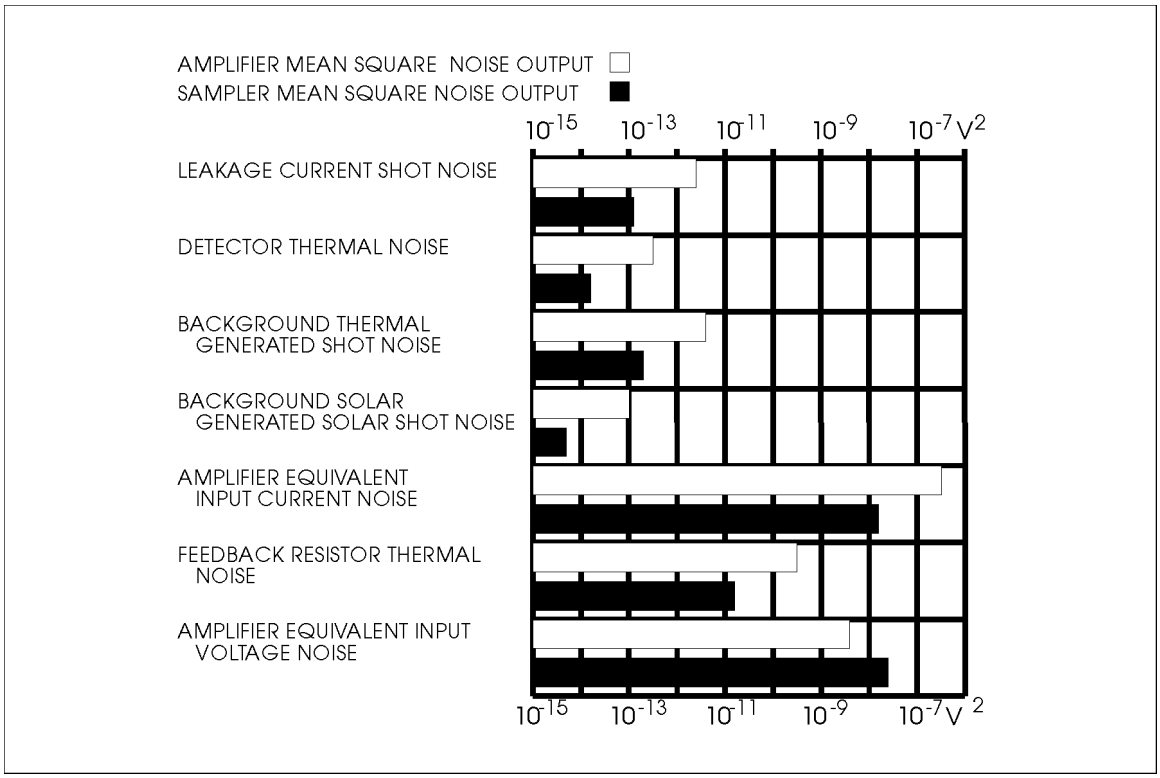


**Figure 11**. Amplifier and sampler noise outputs due to various sources.

- THE RETURN PULSE GENERATES A 0.16V SIGNAL

| • NOISE PERFORMANCE: | AMPLIFIER OUTPUT | SAMPLER OUTPUT |
|---|---|---|
| TOTAL RMS NOISE | $5.657 \times 10^{-4}$ | $2.074 \times 10^{-4}$ |
| THE VOLTAGE SIGNAL-NOISE RATIO | 283 | 772 |

- WE HAVE IGNORED 1/f NOISE IN THIS ANALYSIS BUT THE SAMPLING CIRCUIT STRONGLY SUPPRESSES IT

- AN EXPERIMENTAL CHARGE SENSITIVE AMPLIFIED IS BEING CONSTRUCTED.

**Figure 12.** Charge sensitive amplifier conclusions.

**Transimpedance Amplifier**

Transimpedance amplifiers utilize high open-loop gain with negative feedback to achieve low input impedance and wide bandwidth. This configuration is appropriate for linear wide-bandwidth preamplification of high impedance current sources with substantial parallel capacitance such as photovoltaic optical detectors.

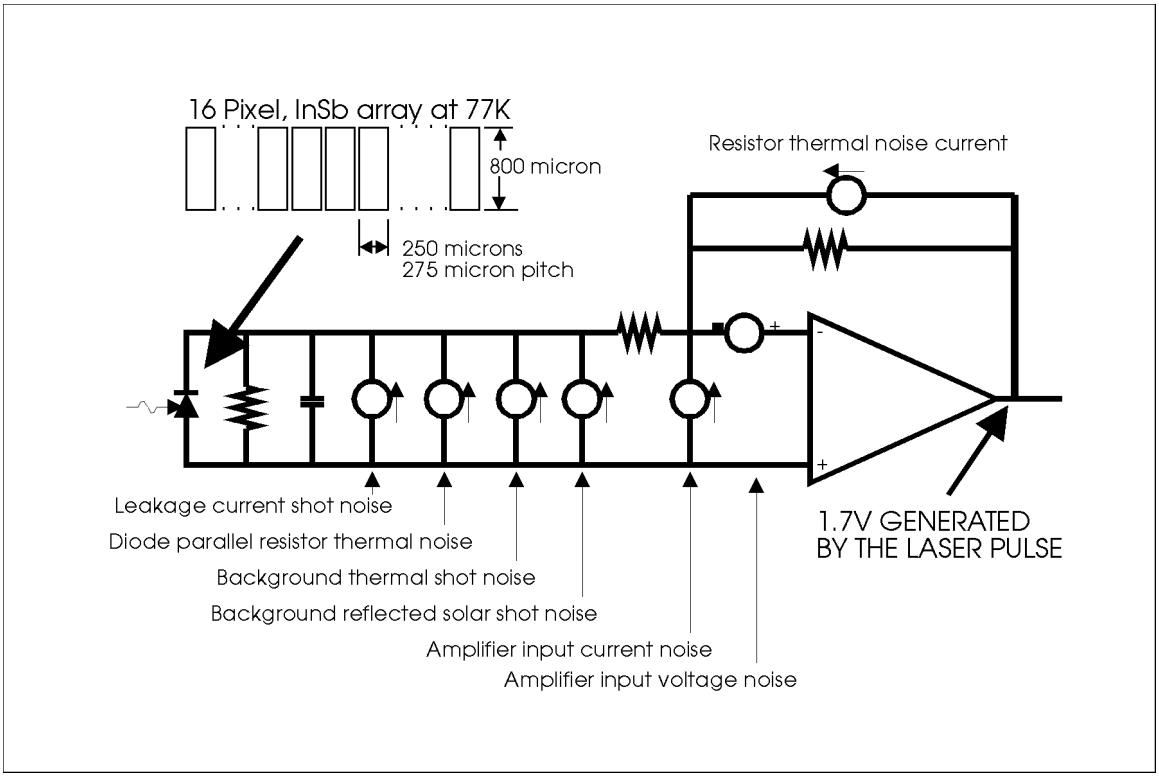


**Figure 13.** Noise model of transimpedance amplifier and detector.

Figure 13 is a schematic noise model of the transimpedance amplifier and detector. The amplifier noise sources are lumped into an equivalent input current shot noise that flows into the inverting input, an equivalent thermal noise voltage which is applied to the inverting input, and the thermal noise current of the feedback resistor. As shown in the charge-sensitive amplifier analyses, detector noise sources from background photons are not dominant and are therefore ignored. The SPICE simulation of Figure 14, predicts the transient response to a pulse at the expected CALIOPE input levels of Figure 15. As expected, the transimpedance gain is equal to the value of the feedback resistance. The output pulse risetime is determined by the detector capacitance and the detector series resistance. A reduction in either of these parameters yields more temporal bandwidth.

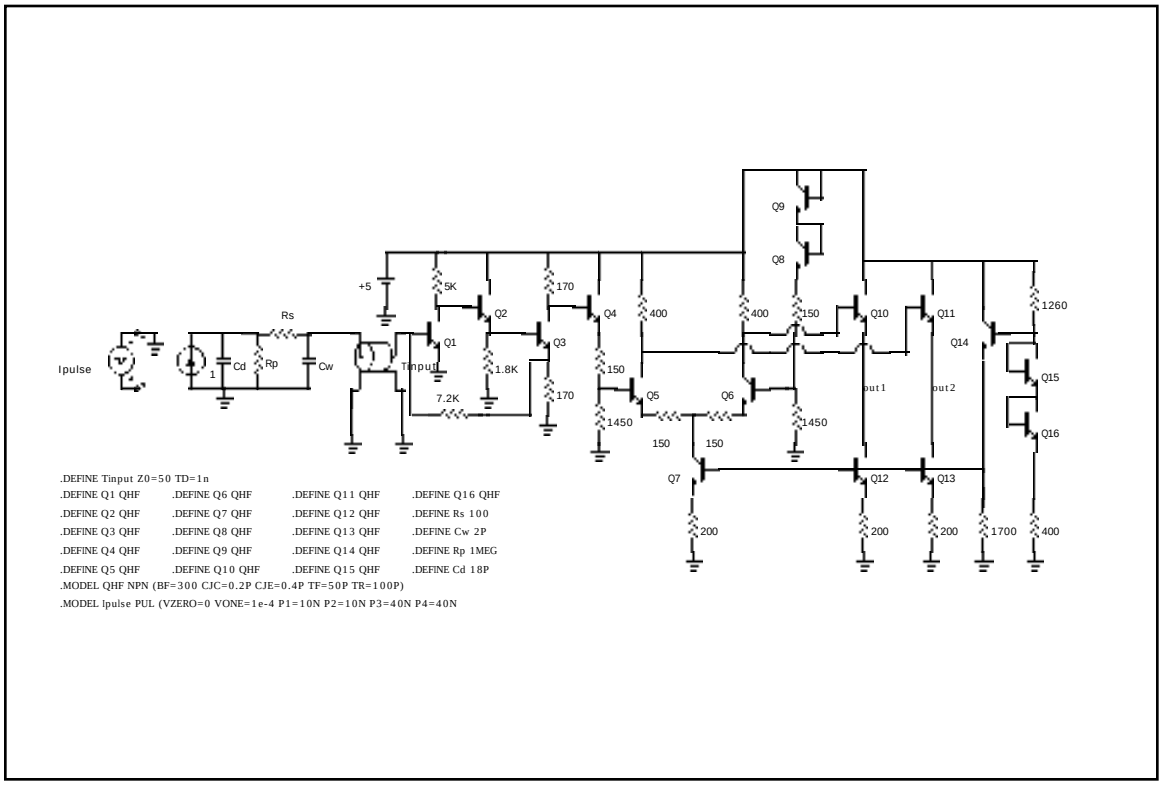


**Figure 14.** SPICE model of transimpedance amplifier and detector.

The SPICE preamplifier output noise voltage spectrum appears in Figure 16. The high frequency noise peaking is due to the shunting of the preamplifier feedback signal to ground by the detector capacitance. This increases the voltage gain of the amplifier for the lumped equivalent noise voltage generator. Fortunately, the linear amplifier is followed by a relatively wide aperture-time integrator which reduces the bandwidth and the high frequency noise peaking has minimal effect on overall system noise.

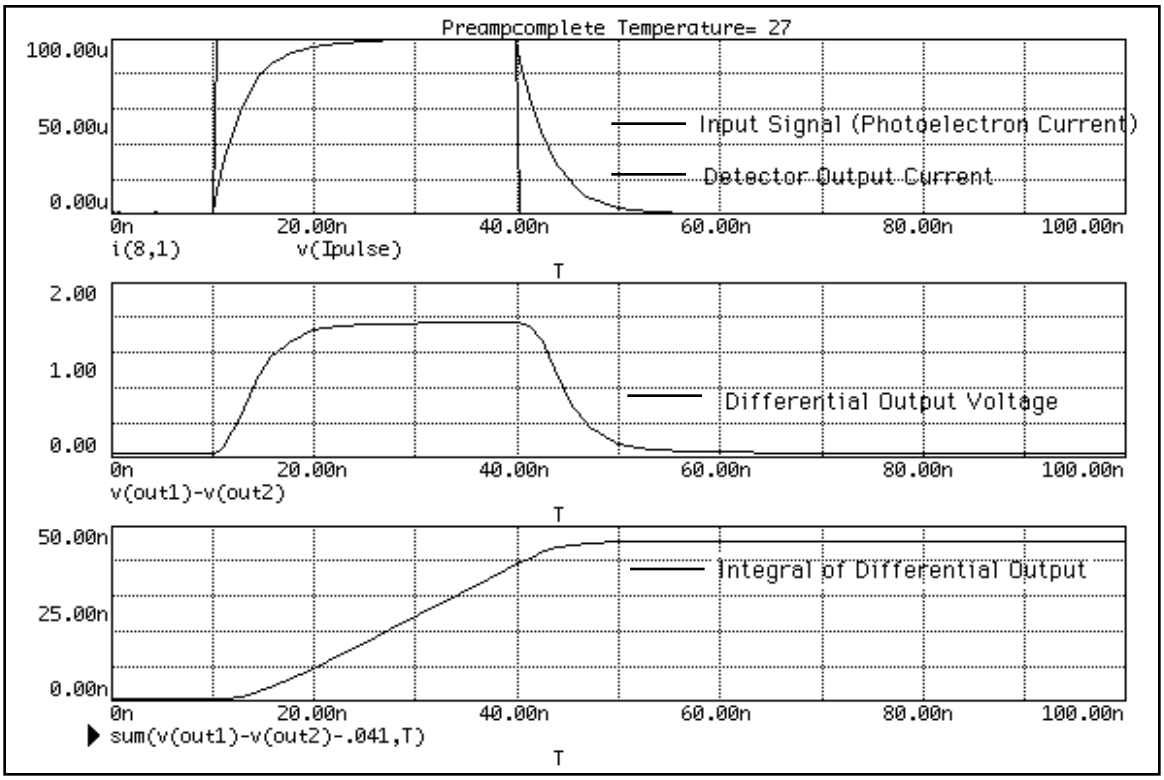


**Figure 15.** Pulse response from SPICE analyses.

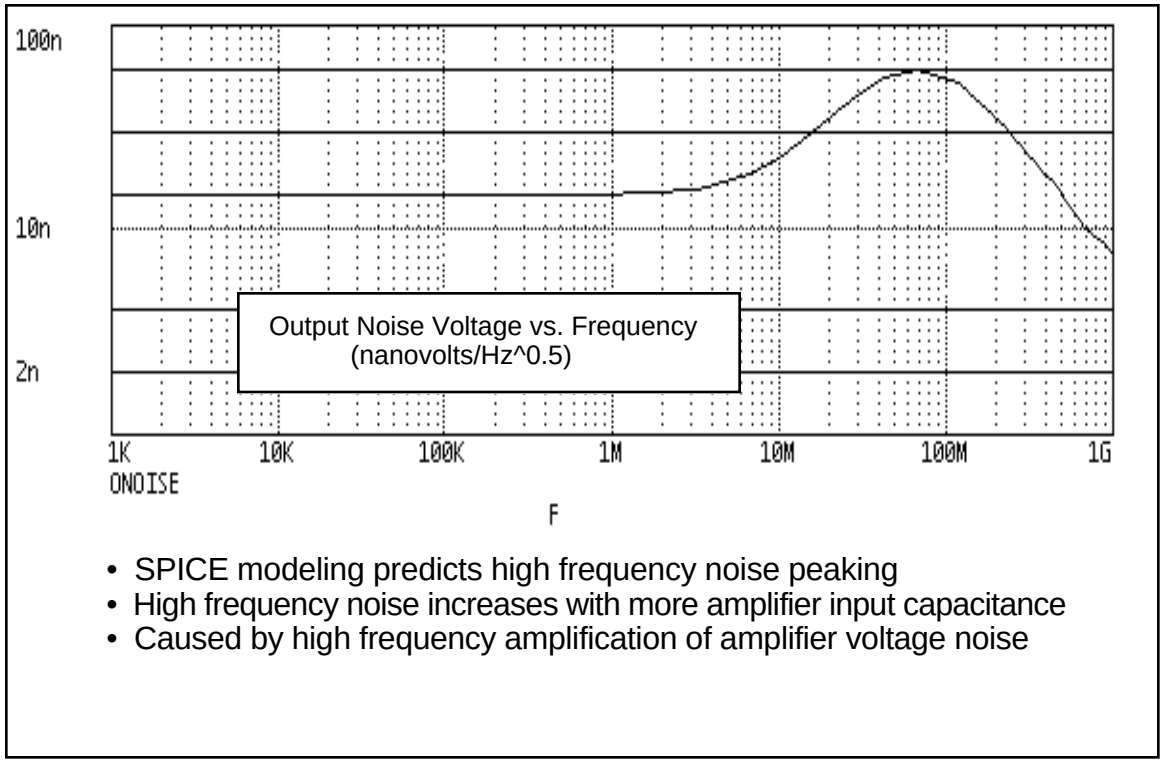


**Figure 16.** SPICE model of amplifier output noise voltage spectrum.

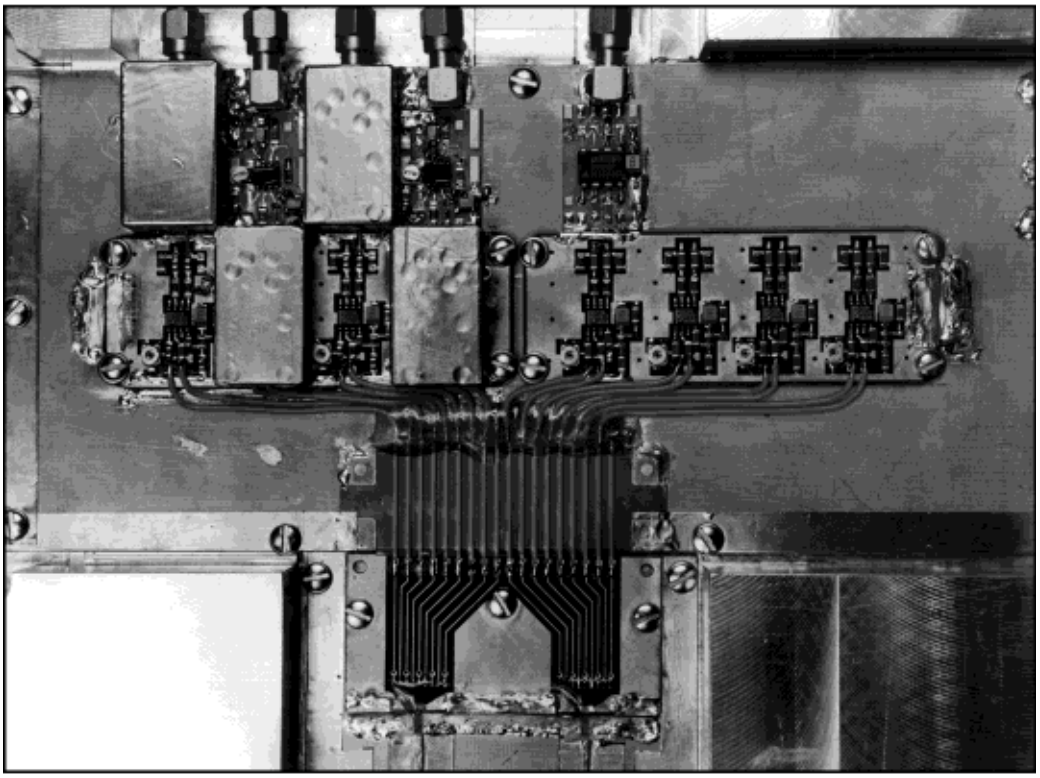

15-K/1248-02

**Figure 17.** Brassboard of multiple channel transimpedance amplifier.

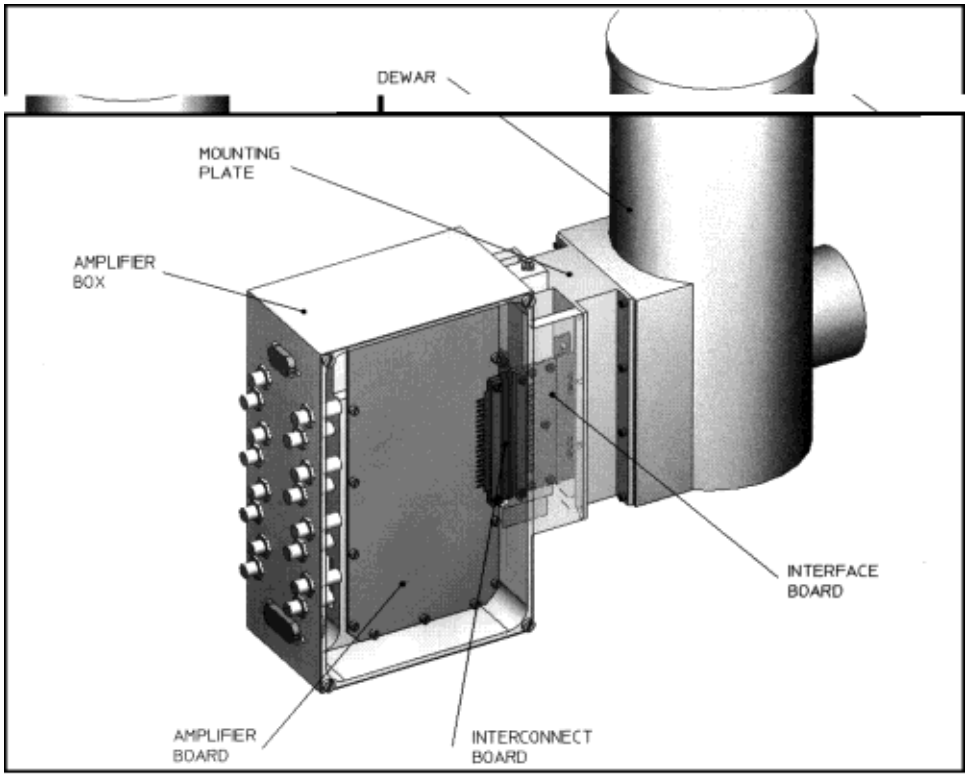


**Figure 18.** Transimpedance amplifier interfaced to detector array dewar.

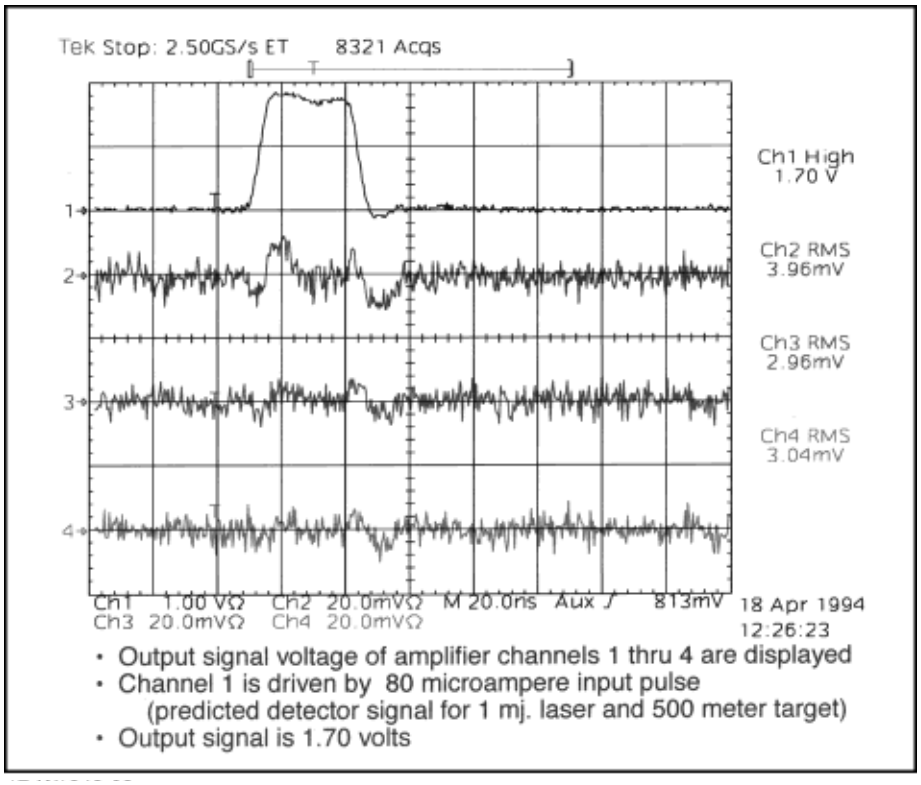


**Figure 19.** Transimpedance amplifier brassboard response to simulated detector signal.

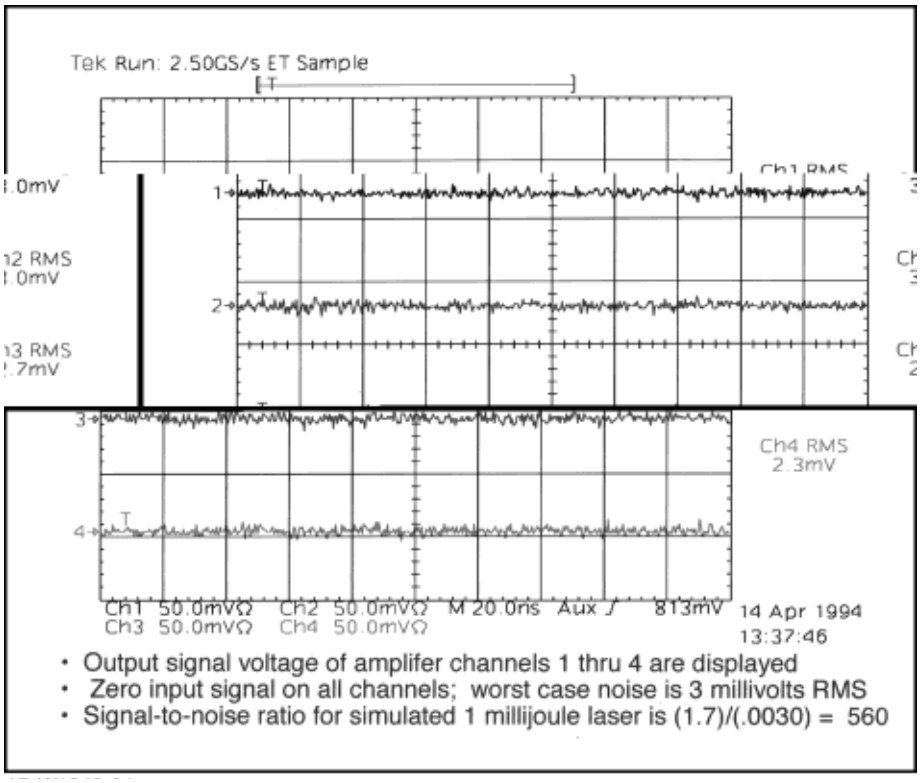


**Figure 20.** Transimpedance amplifier brassboard output noise voltage data with S/N calculation.

A multi-channel brassboard of the amplifier is shown in Figure 17. A CAD rendering of the amplifier packaging and the interface to the cooled detector array appears in Figure 18.

The output rms. noise voltage with no input signal and the differential output voltage for a theoretical CALIOPE test input current pulse have been measured with standard laboratory test equipment. Oscilloscope trace data appears in Figure 19 and Figure 20. The empirical data is comparable to the SPICE predictions. The output signal level for a 80 microampere amplitude input pulse following post-amplification is 1.70 volts and the worst-case rms. noise level for four channels is 3.0 millivolts. This data gives a signal-to-noise ratio of 560 prior to integration. This performance is expected to increase by a factor of two to four after integration.

Two approaches are in progress to obtain the integral of the transimpedance amplifier output signal. The first approach is to use a commercial analog boxcar integrator system. This choice offers expediency and a reduced data bandwidth. Temporal details of the output and return pulses are not retained. The second approach is to use a high speed digitizer to digitize the output pulse shape and digital signal processing to extract the integrated energy signal. The data sampling rate, analog-to-digital converter bit resolution, memory capacity, and processing time issues of this approach are challenging, but the potential reward is an increased signal-to-noise ratio. Digital filtering techniques may allow removal of potential systematic noise or improved rejection of 1/f noise. Digital signal processing also offers more adaptability in software to a variety of system applications. Conclusions regarding the transimpedance amplifier are summarized in Figure 21.

CONCLUSIONS AND COMMENTS ON THE TRANSIMPEDANCE AMPLIFIER

DRIVING THE BRASSBOARD WITH A SIMULATED RETURN PULSE
GENERATES A 1.70V SIGNAL AT THE POST-AMPLIFIER OUTPUT

| NOISE PERFORMANCE: | AMPLIFIER OUTPUT | SAMPLER |
|---|---|---|
| TOTAL RMS NOISE | $3.0 \times 10^3$ | NOT MEASURED |
| THE VOLTAGE SIGNAL-TO-NOISE RATIO | 560 | NOT MEASURED |

RMS NOISE WAS CALCULATED FROM A 200 NANOSECOND DATA SEGMENT WHICH REJECTS 1/f NOISE. DSP INTEGRATION WITH BASELINE SUBTRACTION ALSO REJECTS 1/f NOISE.

MULTIPLE HIGH SPEED SAMPLES FOR THE INTEGRATED ENERGY CALCULATION IMPLIES A SIGNAL-TO-NOISE MULTIPLICATION EQUAL TO THE SQUARE-ROOT OF THE NUMBER OF SAMPLES
~4X (MIN) = 2000

**Figure 21.** Transimpedance amplifier conclusions.


## Acknowledgment

This work was performed under the auspices of the U.S. Department of Energy by Lawrence Livermore National Laboratory under Contract No. W-7405-ENG-48.

***Technical Information Department*** • Lawrence Livermore National Laboratory
University of California • Livermore, California 94550